Yield Displacement Charts for performance-based seismic design

Enrique Hernandez Montes (emontes@ugr.es)
Universidad de Granada https://orcid.org/0000-0001-6068-1264

María L Jalón
University of Granada Superior Technical School of Roads Channels and Ports Engineering: Universidad de Granada Escuela Tecnica Superior de Ingenieria de Caminos Canales y Puertos

Juan Chiachio
University of Granada Superior Technical School of Roads Channels and Ports Engineering: Universidad de Granada Escuela Tecnica Superior de Ingenieria de Caminos Canales y Puertos

Luisa María Gil-Martín
University of Granada Superior Technical School of Roads Channels and Ports Engineering: Universidad de Granada Escuela Tecnica Superior de Ingenieria de Caminos Canales y Puertos

Research Article

Keywords: Performance-based design, yield displacement, yield frequency spectra, preliminary design

Posted Date: April 15th, 2022

DOI: https://doi.org/10.21203/rs.3.rs-1439436/v1

Abstract

A new methodological concept is presented for seismic design, called Yield Displacement Charts (YDC). As with its predecessors, the Yield Point Spectra (YPS) and the Yield Frequency Spectra (YFS), the YDC takes advantage of the simple features of yield displacement (uy), to use uy in a performance-based design versus a force-based period-dependent approach. A self-contained and comprehensive approach to YPS and YFS is presented, enabling the novel aspect of the YDC to be introduced: a tool for a multi-performance objective design that only depends on the location of the structure. Once the YDC has been calculated for a particular place, it can be used for the preliminary design of any structure. For a given value of the yield displacement, the YFS is obtained from the YDC. The suitability of the methodology proposed is illustrated by using a simple case study for a concrete bridge column.

Introduction

Preliminary design is the first step in a seismic design process (Aschheim et al. 2019) (Palermo et al. 2016). The accuracy of a preliminary design is of the greatest importance. Due to the fact that, in most structures, displacement caused by earthquakes is mainly in the first mode of vibration, preliminary seismic designs are usually based on the response of single degree of freedom systems.

The first section of the article is dedicated to describing, in a mathematically compact and simple way, the response of a single degree of freedom system in the linear elastic domain and in the plastic domain. The second section presents the seismic hazard curve (peak ground acceleration -PGA- versus probability of occurrence), particularized for Granada –Spain-. PGA has been chosen to measure the intensity of the ground motion, despite the existence of better period-dependent describers (e.g. the spectral acceleration, $S_a(T)$, (Luco and Bazzurro 2007)) and other non-period-dependent describers (e.g. peak ground velocity or peak ground displacement (Palermo et al. 2014)).

The main reason for not using a period-dependent variable is that yield displacement is going to be used in the presentation of the Yield Displacement Charts (YDC), the main novel aspect of this work. The use of the period has been avoided throughout the article since the period loses its physical meaning in the plastic range.

Several spectral representations of the seismic demand of single degree of freedom (sdof) systems are available in the literature. The most common representation is pseudo-acceleration versus the period of the sdof system. The yield point spectra (YPS) uses yield displacement (u_y) as an alternative to the period (T) (Mark Aschheim and Black 2000). The great advantage of yield displacement is that, for a given structural configuration, it is a more stable parameter than the period, which is an important property in preliminary designs. The properties of yield displacement are explained in the third section of this paper.

Performance-based seismic designs that consider several performance objectives corresponding to different seismic hazard levels are now more commonly used, and they are recommended in (SEAOC 1999), (Fib 2012). In this context, Yield Frequency Spectra (YFS) (Vamvatsikos and Aschheim 2016) are

regarded as an efficient tool for dealing with this type of analysis. YFS are a graphical representation that link the mean annual frequency/rate (MAF) of exceeding a ductility threshold (i.e. a performance objective) with the system yield strength coefficient (C_y). YFS are plotted for a given yield displacement (u_y), and they allow the demand of the system for different performance objectives to be visualized. The fifth section deduces the YFS from the theoretical framework of the conditional probability, and it presents the Yield Displacement Charts (YDC). Yield Displacement Charts (YDC) pursue the same objective as the YFS, but they are obtained by considering yield displacement as a variable, so the result is a performance-based seismic design tool that only depends on the geographical location of the structure. The YDC is calculated for Granada city in the sixth section. Finally, a simple example of structural design is developed.

The Response Of The Single Degree Of Freedom System

The time-history displacement response, $u(t)$, of a linear-elastic SDOF system, for a fixed value of damping, subjected to a given ground motion, $\ddot{u}_g(t)$, is characterized by only one variable, which is usually period T. From this period, $\omega = 2\pi/T$ and $k = \omega^2 m$ can be computed, with k as the initial stiffness, m the mass and ω the natural circular frequency of the system (see Fig. 1). The maximum displacement of a linear-elastic SDOF for a given ground motion is called elastic spectral displacement $S_d = \max[u(t)]$, for which the SDOF develops an elastic force $F_e = k\, S_d$. Typically, this elastic force is presented in the literature as being divided by mass m, and then it is called *spectral pseudo-acceleration*: $S_a = F_e/m$. From the simple relationships above, it can be demonstrated that $S_a = \omega^2 S_d$. Since T characterizes the SDOF response for a given ground motion, all the variables defined above can be expressed as functions of T, i.e.: $S_a(T)$, $S_d(T)$ and $F_e(T)$. For example, the (pseudo-acceleration) response spectrum of a ground motion can be represented by $S_a(T)$ versus T, as shown in Fig. 2.

In structural engineering design, the seismic action is not unique (note that Fig. 2 corresponds only to one seismic accelerogram, $\ddot{u}_g(t)$). Furthermore, a probabilistic treatment of the seismic action is required. Simple envelope approximations of uniform-hazard response spectra derived from probabilistic seismic hazard analysis (PSHA, Cornell 1968) are used in professional standards for structural design purposes: the *design spectra*. For a SDOF system of period T and mass m, the design spectrum gives the maximum elastic force that can be developed by the SDOF system, $S_a(T)m$, for a certain probability of occurrence, e.g. 10% in 50 years.

Likewise, a non-linear SDOF system modeled as elasto-plastic can be characterized by only two variables, usually C_y and u_y, with u_y as the yield displacement and C_y as the yield strength coefficient defined as $C_y = F_y/mg$ where F_y is the yield strength (see Fig. 3). Note the absence of a period in this characterization, which is defined via C_y and u_y as

$$T = 2\pi \sqrt{\frac{u_y}{C_y g}}$$

1

If the maximum displacement of this non-linear system for a given ground motion is u_{max} so that if $u_{max} > u_y$, then the maximum displacement is in the plastic range. It is important to note that once the system is in the yield plateau, the main recovery factor of the system in terms of displacement is the cyclical nature of the seismic action itself, whereby the system alternates between unloading/reloading at elastic stiffness (or near-elastic for non-kinematic-hardening hysteresis rules), and it sustains further damage along the yield plateau. In other words, the importance of a period as a performance-prediction variable is limited when the system enters the post-yield range. The reader should be aware that the authors are looking for a simple preliminary design tool, not a complete and comprehensive description of the response.

In the time-history analysis, ductility (μ) is defined as u_{max}/u_y (i.e., ductility demand). Given that demand should not overcome capacity (D < C), it is necessary to ensure that the ductility demanded by the earthquake is at least equal to the ductility capacity in the structure. In other words, when designing for a certain level of ductility, the designer needs to ensure that the structure is going to allow reliable plastic behavior in the areas of (pre-designated) structural detailing where plasticity is going to take place (i.e., ductility capacity). Although it is a little unconventional, for the sake of mathematical completeness, values of μ smaller than 1 are going to be considered (even if they are not proper ductility) in order to also include the cases where u_{max} is smaller than u_y in the study. Even though the SDOF is characterized by one or two variables depending on whether it is linear or elasto-plastic, the (maximum or worst-case) response of the system can be described by only one variable: the maximum displacement, S_d or u_{max}. The inelastic displacement ratio C_1 is defined to relate $S_d(T)$ and u_{max}, so that $u_{max} = C_1 S_d(T)$, FEMA 440(FEMA 2005).

A simple way to describe the intensity of a ground motion is S_d, because it shows, as no other parameter does, the effect of a specific ground motion on an elastic SDOF of period T. Notice that, as mentioned, $S_a = \omega^2 S_d$, lending the same properties of S_d to S_a. As discussed, the strength of this relationship is weakened when entering the non-linear range. This is quantified by the use of inelastic displacement ratios $C_1(C_y, T)$, also known as R-μ-T strength ratio/ductility/period relationships (where R is essentially C_y, see Fig. 3). Since the connection is no longer deterministic, these relationships convey the statistics of inelastic displacement u_{max} for systems of a given C_y and T, typically offering the mean estimate, $\bar{u}_{max}$, for use in tandem with the static pushover (e.g., (FEMA 2005), (EN1998-3 2005)):

$$\bar{u}_{max} = C_{1m}\left(C_y, T\right) S_d(T)$$

2
where C_{1m} is the mean inelastic displacement ratio function for a given C_y and T.

The predictive ability of S_d and S_a, the intensity measures (IMs) within the framework of Performance-Based Earthquake Engineering (Cornell and Krawinkler 2000) can be characterized by implementing the associated dispersion of the distribution of $C_1(C_y,T)$, as offered by e.g. (Vamvatsikos and Cornell 2006) or (Ruiz-García and Miranda 2007). This is the so-called IM efficiency (Luco and Cornell 2007) and the lower the dispersion, the higher the efficiency and associated predictive capability. The issue of IM sufficiency also arises (Nicolas Luco and Cornell 2007), which characterizes the capability of S_d and S_a to render the distribution of $C_1(C_y,T)$, or equivalently of $u_{\max}$ conditioned on S_d or S_a, independent of other seismological characteristics.

Sufficiency is a particularly useful property, as it negates (or generally reduces) bias when assessing performance (see Section 4). $S_a(T)$ is moderately efficient and sufficient, but clearly imperfect whenever large excursions into non-linearity or significantly higher-mode effects are involved (e.g. (Luco and Bazzurro 2007). At the same time, $S_a(T)$ is clearly better than peak ground acceleration *PGA* (e.g., (Kazantzi and Vamvatsikos 2015)) for everything but the shortest periods, in which the two parameters are practically identical. Nevertheless, in the Yield Displacement Charts (YDC) presented, the authors are going to use *PGA* as the intensity measure, emphasizing the fact that it is not period dependent, which makes it more versatile than $S_a(T)$ at the cost of reducing efficiency and sufficiency. The authors believe this tradeoff is acceptable for practical design applications, where simplicity is important, and conservativeness can be added as needed to make up for the probabilistic deficiencies of *PGA*.

The Seismic Hazard

The intensity of the ground motion at a certain site can be measured by IMs that, among other parameters, may be represented, as mentioned, by peak ground acceleration *PGA* or pseudo-acceleration $S_a(T)$. The level of ground motion intensity expected at the site is associated to a certain frequency/rate of occurrence, and this is calculated by using the total probability theorem, combining several probabilistic distributions, and conveying information about the seismic sources (faults), the site (e.g., soil type), and the source-to-site propagation (Baker 2013). This is known as probabilistic seismic hazard analysis (PSHA), and a representation of the intensity of ground motion, measured by the *PGA* versus its MAF is the seismic hazard curve $\lambda(PGA)$.

The site-specific seismic hazard curve, $\lambda(PGA)$, is obtained by using the seismic source model (Giardini et al. 2014) as estimated by (EFEHR, 2021) for Granada (latitude 37.18̊, longitude − 3.60̊), considering a soil with an average shear wave speed in the upper 30m of V_{s30}=250m/s. The seismic hazard curve is approximated by using a continuous smooth interpolation curve (splines), as shown in Fig. 4.

The Use Of Yield Displacement For Design

Preliminary design usually begins with the period of the first mode of the structure, or a combination of some of the modes, which is known as the equivalent single degree of freedom (ESDOF) system (Aschheim et al. 2019).

As an alternative, some displacement-based methods for seismic design (e.g. (Mark Aschheim and Black 2000) and (Paulay 2002)) use an estimate of the yield displacement for establishing values of the base shear strength. The main advantage of yield displacement, instead of the period, is that it is very stable for stiffness changes. This stability has been confirmed at both a sectional level and at a global system level (e.g. Hernández-Montes and Aschleim 2003, Priestley et al. 2007, Hernández-Montes et al 2019). As an illustration of this feature, Fig. 5 shows the base shear resultant of two buildings subjected to a monotonic lateral force profile, as a function of the displacement at the roof. The only difference between the two models is the amount of reinforcement. Figure 5 shows that the yield displacement (D_y) remains stable (gray bar in Fig. 5).

So, the stability of the yield displacement converts it into a key performance variable for the seismic design of structures (Aschheim and Montes, 2003). Estimations of the yield displacement for several structural systems and different cross-sections can be found in Chap. 9 of (Aschheim et al. 2019).

Yield Displacement Charts

The performance of a SDOF system under a seismic action, formulated in terms of conditional probability, can be described as the MAF (λ) by which the maximum displacement (u_{max}) exceeds a certain limit displacement (δ):

$$\lambda\left(\delta \mid C_y, u_y\right) = P\left[u_{\max} > \delta \mid C_y, u_y\right] = \int_0^{\infty} P\left[u_{\max} > \delta \mid PGA, C_y, u_y\right] \left|\mathrm{d}\lambda(PGA)\right|$$

3

where λ(•) denotes the MAF of its argument, $P[u_{max} > \delta|PGA,C_y,u_y]$ is the probability of u_{max} exceeding a threshold δ conditioned on the yield strength coefficient (C_y), the yield displacement (u_y), as well as on the peak ground acceleration (*PGA*). The second term inside the integral is the differential of the *PGA* seismic hazard curve, the latter being the function of the MAF of exceeding a given value of *PGA*, λ(*PGA*). Note that, by assuming the sufficiency of the *IM* (here *PGA*), any conditioning on seismological characteristics, such as magnitude or distance has been dropped. This is a key assumption of the conditional approach (Bazzurro et al. 1998) that allows this standard treatment of Performance-Based Earthquake Engineering.

The integral above can be solved numerically as:

$$\lambda\left(\delta \mid C_y, u_y\right) = \sum_{j=1}^{N} P\left[u_{max} > \delta \mid PGA_j, C_y, u_y\right] \Delta\lambda\left(PGA_j\right)$$

4

where $\Delta\lambda\,(PGA_j) = \lambda\,(PGA_j) - \lambda\,(PGA_{j+1})$, with $PGA_{j+1} > PGA_j$.

Since the integral (or summation) is calculated over the IM, here, with the IM as *PGA*, the variable *PGA* disappears when the integral is completed.

For a particular system, given by C_y and u_y, the above equation can be represented as a curve of λ-δ, see Fig. 6a, where it can be observed that when displacement threshold values (δ) increase, the probability that u_{max} exceeds δ decreases. Additionally, C_y can be considered to be a variable. Curves of constant value of C_y can be plotted together, see Fig. 6b. It can be observed that as the value of C_y increases, the probability of exceedance decreases.

The limit displacement (δ) divided by u_y is the ductility threshold, μ (i.e. $\mu = \delta/u_y$). If the horizontal axis of Fig. 6b is changed from δ to μ (see Fig. 6c) a new representation, known as the Yield Frequency Spectra (YFS), is obtained (Vamvatsikos and Aschheim 2016).

The YFS relate the probability of exceedance of a given displacement threshold at a certain place (where the seismic hazard and the soil characteristics are known) for an elasto-plastic sdof system, half-defined, because the yield displacement u_y has to be known.

As already mentioned, the yield displacement u_y is very stable for stiffness changes, which makes YFS the perfect tool for starting a multi-objective design.

By forcing u_y to be a variable, a new design tool can be created: The Yield Displacement Charts (YDC), see Fig. 7.

For a series of values of C_y and u_y within a feasible range, the resulting curves λ-δ provide charts that are only dependent on the location of the structure, i.e., the charts are independent of the characteristics of the system. In the next step, once the value of u_y for a particular structural system has been discovered (Chap. 9 of (Aschheim et al. 2019)), a YFS is obtained from the YDC. The designer is able to obtain the base shear for different performance objectives from the YFS.

Unlike the work of (Ruiz-García and Miranda 2007), in the method presented here, the YDC is computed directly from a particular earthquake database instead of using the statistical information from the previously deduced maximum inelastic displacement (Ruiz-García and Miranda 2003). Thus, from Eq. (4), the values of λ as function of C_y and u_y are obtained for a given place (meaning that soil conditions and seismic hazard are constant).

Implementation Of Yield Displacement Charts

For a comprehensive suite of elastic-hardening bilinear SDOF systems defined by C_y and u_y (see Fig. 3), the maximum displacement values $u_{\max}$ are obtained by using a database of 980 earthquakes. For all the

SDOFs, 5% damping, 3% of post-yield stiffness ratio and elastic stiffness degradation defined by $\alpha = 0.5$ have been considered. The degraded elastic stiffness (k_u) is defined as:

$$k_u = k \left(\frac{u_y}{u_{max}} \right)^{\alpha}$$

5

All the ground motions used in this study have been obtained from (RESORCE 2020). No additional corrections were applied to the downloaded ground motion records. The filtering parameters applied in the process of record selection are as follows:

• Records with a magnitude greater than 5 are selected.

• Any source-to-site distance

• Both pulse-like and non-pulse-like motions

• Records with V_{S30} between 180 and 360 m/s.

• Both of the horizontal component recordings available are considered.

As a sample, Fig. 8 shows the u_{max} obtained for the 980 ground motions (490 recordings times with two components each) considered for the case of $C_y = 0.3$ and $u_y = 0.025$m. A high dispersion is observed for $PGA > 0.2$g, where high structural nonlinearity appears, which is captured by few records. Specifically, there are 952 motions in $0 < PGA \leq 0.2$g whereas there are only 28 motions in $0.2\text{g} < PGA \leq 0.9$g. Employing scaled ground motion can better populate the higher range of response, but this is at the expense of introducing issues of scaling bias, given the use of *PGA*. Accounting for the above, the authors preferred to continue using with unscaled motions.

The results are treated using cloud analysis (Cornell et al. 2002). The cloud of data u_{max} versus *PGA*, see Fig. 8 left, are related by using linear regression in the logarithmic space: $u_{max}=a \cdot PGA^b$, or by applying logarithms: $\text{Ln}[u_{max}] = \text{Ln}[a] + b \cdot \text{Ln}[PGA]$. The constants are calculated by using regression analysis for each particular system (i.e. C_y and u_y are given), see Fig. 8 on the right for the particular case that is being shown, for which Ln[a] = − 2.12 and b = 0.92, with 0.6 as the standard deviation, σ.

The regression analysis provides, the mean and the standard deviation for each value of PGA. In this sample, the mean value is $\mu = -2.12 + 0.92 \cdot \text{Ln}[PGA]$ and $\sigma = 0.6$. Assuming that $\text{Ln}[u_{max}]$ follows a normal distribution, see Fig. 8 on the right, then u_{max} follows a lognormal distribution. Note that the lognormal distribution characterizes variables with a tendency to produce frequent extremely high values, and it is often used in earthquake engineering, especially when modelling seismic demand.

The lognormal cumulative distribution function gives the probability of occurrence of a given displacement threshold, say δ, for given values of PGA, C_y, and u_y: i.e. $P[u_{max} \leq \delta \mid PGA, C_y, u_y]$. Figure 9 shows the lognormal cumulative density function for the sample case (i.e., C_y = 0.3 and u_y = 0.025m) and for six different values of PGA.

Finally, considering that $P[u_{max} > \delta \mid PGA_j, C_y, u_y] = 1 - P[u_{max} \leq \delta \mid PGA_j, C_y, u_y]$, the integrand of the Eq. (3) is obtained.

The λ-δ curve (see Fig. 6a) is obtained by numerically applying Eq. (4). The seismic hazard curve λ(PGA) used in Eq. (4) is the one shown in Fig. 4 (i.e., for the case of Granada).

The displacements (u_{max} and δ) are divided by the yield displacement (u_y) obtaining the ductility demand and the ductility threshold (i.e., a threshold limit in terms of ductility, also called ductility capacity), respectively. Figure 10 shows the curve λ-μ for the sample system (u_y=0.025m and C_y=0.3) and the location in Granada.

The above methodology is applied for different SDOF systems after the selection of values of C_y (0.1, 0.2, 0.3, 0.4, 0.5, 0.6, 0.7, 0.8, 0.9, 1) and u_y (0.025 m, 0.05 m, 0.1 m). The obtained u_{max} values versus the *PGA* are represented in Fig. 11, and the obtained Yield Displacement Chart for the city of Granada is originally shown in Fig. 12.

Example Of The Design Approach

In order to illustrate a design case with multiple performance objectives based on yield displacement, a simple example has been developed, see Fig. 13. The example consists of a single-column pier of a highway bridge located in Granada (Spain). In accordance with (EN1998-1 2004), the design has to fulfill the two following performance objectives:

1. The life safety (LS) requirement, associated to a probability of exceedance of 10% in 50 years (return period of 475 years), i.e. $\lambda_{LS} = -\ln(1 - 0.1)/50 = 2.11 \times 10^{-3}$ years^{-1}.

2. The damage limitation (DL) requirement, associated to a probability of exceedance of 10% in 10 years (return period of 95 years), i.e., λ_{DL} = 0.0105 years^{-1}.
The effective yield curvature (ϕ_y) for circular column cross-sections is estimated (Hernández-Montes and Aschheim 2003) as:

{\varphi }_{y}=2.3 \frac{{ϵ}_{y}}{d}
6
where ε_y is the yield strain of the reinforcing steel and d is the depth of the extreme tension reinforcing bar. For steel B-400 the characteristic strength is f_{yk}=400 MPa, leading to ε_y = 400/200000 = 0.0020. The

column has a circular cross section with a diameter of 1.2 m. The cover chosen is2.5 cm, thus d = 1.2 − 0.05 = 1.15 m. The above results in an effective yield curvature ϕ_y = 0.00397 rad/m.

The yield displacement (u_y) for a cantilever column subjected to a lateral load when shear deformation is neglected can be deduced by integrating the curvature along the length of the column twice with $\phi = \phi_y$ for x = 0, see Fig. 14 and Eq. 7.

{\varphi \left(x\right)=\varphi }_{y}\frac{L-x}{L}\to {u}_{y}=\int \left(\int \varphi \left(x\right)dx\right)dx= {\varphi }_{y}{\left.\left(\frac{{x}^{2}}{2}-\frac{{x}^{3}}{6L}\right)\right|}_{0}^{L}={\varphi }_{y}\frac{{L}^{2} }{3}=0.048 m
7

The DL drift ratio, assumed to be of 2%, results in a displacement of 0.02•6.00 m = 0.12m, with the ductility associated to this displacement as μ = 0.12/0.048 = 2.5.

The target ductility for LS has been chosen following (Mander 1983). According to Figs. 7.10 and 7.11 of (Mander 1983), the ductility capacity goes from 3.0 to 10.0, depending on the confinement and the longitudinal steel ratio. A value of 5.0 has been adopted here for the preliminary design.

The YFS for u_y = 0.048 m (see Eq. 7) is calculated by the interpolation between u_y = 0.025 m and u_y = 0.05 m in the YDC (Fig. 12). This YFS and the two performance objectives are represented in Fig. 15. Both performance objectives were expressed in terms of target MAF and ductility: a ductility of 2.5 associated to a MAF of 0.0105 years^{-1} (which, from Fig. 15, leads to C_y = 0.51) and a ductility of 5.0 associated to a MAF of 2.11×10^{-3} years^{-1} (for which C_y = 0.49). The highest value of C_y is the design value, that in this case is governed by the first performance objective.

As the pier is subjected to a dead load of 6500 kN (see Fig. 13), the column has to be designed for a lateral seismic load of 0.51·6500 kN = 3315 kN.

Conclusions

The Yield Displacement Chart (YDC) approach is introduced. YDCs are based on the fact that the yield displacement remains constant with changes in stiffness, at the sectional level and at the structural level. By further replacing the spectral acceleration basis with a peak ground acceleration one, the YDC requires more compact hazard and response information, compared to the Yield Frequency Spectra (YFS). YDC is essentially a property of a given site, in this sense the engineers can use the same YDC for all the design purposes within the site. Despite the loss of some efficiency and sufficiency, this $S_a(T_1)$-by-*PGA* substitution offers increased practicality and conceptual simplicity, turning YDC into a unique tool for performance-based design.

Declarations

Acknowledgments

This work is part of the HYPERION project (https://www.hyperion-project.eu/). HYPERION has received funding from the European Union's Framework Programme for Research and Innovation (Horizon 2020) under grant agreement no. 821054. The content of this publication is the sole responsibility of the authors and does not necessarily reflect the opinion of the European Union.

The authors would like to thank Prof. Dimitrios Vamvatsikos from the National Technical University of Athens for his valuable discussion during the development of his article.

The authors declare that there is no conflict of interest.

References

1. Aschheim M, Montes EH (2003) The Representation of P-Δ Effects Using Yield Point Spectra. Eng Struct 25(11). https://doi.org/10.1016/S0141-0296(03)00106-8
2. Aschheim M, Black EF (2000) Yield Point Spectra for Seismic Design and Rehabilitation. Earthq Spectra 16(2):317–335. https://doi.org/10.1193/1.1586115
3. Aschheim M, Hernández-Montes E (2019) Design of Reinforced Concrete Buildings for Seismic Performance: Practical Deterministic and Probabilistic Approaches. CRC Press. https://www.crcpress.com/Design-of-Reinforced-Concrete-Buildings-for-Seismic-Performance-Practical/Aschheim-Hernandez-Montes-Vamvatsikos/p/book/9780415778817 Taylor & Francis
4. Baker JW (2013) "Probabilistic Seismic Hazard Analysis. White Paper Version 2.0." Vol. 79. Stanford CA. https://web.stanford.edu/~bakerjw/Publications/Baker_(2013)_Intro_to_PSHA_v2.pdf
5. Bazzurro, Paolo CA, Cornell N, Shome, Carballo JE (1998) "Three Proposals for Characterizing MDOF Nonlinear Seismic Response." *Journal of Structural Engineering* 124 (11): 1281–89. https://doi.org/10.1061/(asce)0733-9445(1998)124:11(1281)
6. Cornell CA, Jalayer F, Hamburger RO, Foutch DA (2002) Probabilistic Basis for 2000 SAC Federal Emergency Management Agency Steel Moment Frame Guidelines. J Struct Eng 128(4):526–533
7. Cornell CA (1968) Engineering Seismic Risk Analysis. Bull Seismol Soc Am 58(5):1583–1606
8. Cornell CA, Krawinkler H (2000) "Progress and Challenges in Seismic Performance Assessment." https://apps.peer.berkeley.edu/news/2000spring/performance.html
9. EN1998-1 (2004) *Eurocode 8: Design of Structures for Earthquake Resistance -Part 1: General Rules, Seismic Actions and Rules for Buildings. EN1998-1*. Brussels
10. EN1998-3 (2005) *Eurocode 8: Design of Structures for Earthquake Resistance - Part 3: Assessment and Retrofitting of Buildings*. Brussels
11. FEMA (2005) "Improvement of Nonlinear Static Seismic Analysis Procedures, FEMA 440." Washington, D.C
12. Fib (2012) "Probabilistic Performance-Based Seismic Design. Bulletin 68." Lausanne, CH

13. Giardini D, Woessner J, Danciu L (2014) Mapping Europe's Seismic Hazard. EOS 95(29):261–262
14. Hernández-Montes E, Aschheim MA (2019) A Seismic Design Procedure for Moment-Frame Structures. J Earthquake Eng 23(9). https://doi.org/10.1080/13632469.2017.1387196
15. Hernández-Montes E, and M. Aschleim (2003) Estimates of the Yield Curvature for Design of Reinforced Concrete Columns. Magazine of Concrete Research 55(4). https://doi.org/10.1680/macr.2003.55.4.373
16. Hernández-Montes E, Chatzidaki A, Gil-Martin LM, Aschheim M, Vamvatsikos D (2019) A Seismic Design Procedure for Different Performance Objectives for Post-Tensioned Walls. J Earthquake Eng. https://doi.org/10.1080/13632469.2019.1691678
17. Kazantzi AK, and Dimitrios Vamvatsikos (2015) Intensity Measure Selection for Vulnerability Studies of Building Classes. Earthq Eng Struct Dynamics 44(15):2677–2694. https://doi.org/10.1002/eqe.2603
18. Luco N, and P Bazzurro (2007) "Does Amplitude Scaling of Ground Motion Records Result in Biased Nonlinear Structural Drift Responses? Earthquake Eng Struct Dynam 36:1813–1835. https://doi.org/10.1002/eqe.695
19. Luco N, Allin Cornell C (2007) Structure-Specific Scalar Intensity Measures for Near-Source and Ordinary Earthquake Ground Motions. Earthq Spectra 23(2):357–392. https://doi.org/10.1193/1.2723158
20. Mander JB (1983) "Seismic Design of Bridge Piers. PhD Thesis." University of Canterbury. https://www.researchgate.net/publication/34205859_Seismic_design_of_bridge_piers
21. Palermo M, Silvestri S, Gasparini G, Trombetti T (2014) A Statistical Study on the Peak Ground Parameters and Amplification Factors for an Updated Design Displacement Spectrum and a Criterion for the Selection of Recorded Ground Motions. Eng Struct 76:163–176. https://doi.org/https://doi.org/10.1016/j.engstruct.2014.06.045
22. Palermo M, Silvestri S, Landi L, Gasparini G, and Tomaso Trombetti (2016) Peak Velocities Estimation for a Direct Five-Step Design Procedure of Inter-Storey Viscous Dampers. Bull Earthq Eng 14(2):599–619. https://doi.org/10.1007/s10518-015-9829-8
23. Paulay T (2002) A Displacement-Focused Seismic Design of Mixed Building Systems. Earthq Spectra 18(4):689–718. https://doi.org/10.1193/1.1517066
24. Priestley MJN, Calvi GM, Kowalsky MJ (2007) Displacement-Based Seismic Design of Structures. IUSS Press, Pavia
25. "RESORCE." 2020.
26. Ruiz-García J, and Eduardo Miranda (2003) Inelastic Displacement Ratios for Evaluation of Existing Structures. Earthq Eng Struct Dynamics 32(8):1237–1258. https://doi.org/https://doi.org/10.1002/eqe.271
27. ———. "Probabilistic Estimation of Maximum Inelastic Displacement Demands for Performance-Based Design." *Earthquake Engineering & Structural Dynamics* 36 (9): 1235–54. https://doi.org/10.1002/eqe.680

28. SEAOC. “Recommended Lateral Force Requirements & Commentary (Blue Book).” Sacramento, CA
29. Vamvatsikos D, Aschheim MA (2016) “Performance-Based Seismic Design via Yield Frequency Spectra.” *Earthquake Engineering and Structural Dynamics*, no. 45: 1759–78
30. Vamvatsikos D, Allin Cornell C (2006) Direct Estimation of the Seismic Demand and Capacity of Oscillators with Multi-Linear Static Pushovers through IDA. Earthquake Eng Struct Dynam 35(9):1097–1117. https://doi.org/10.1002/eqe.573

Figures

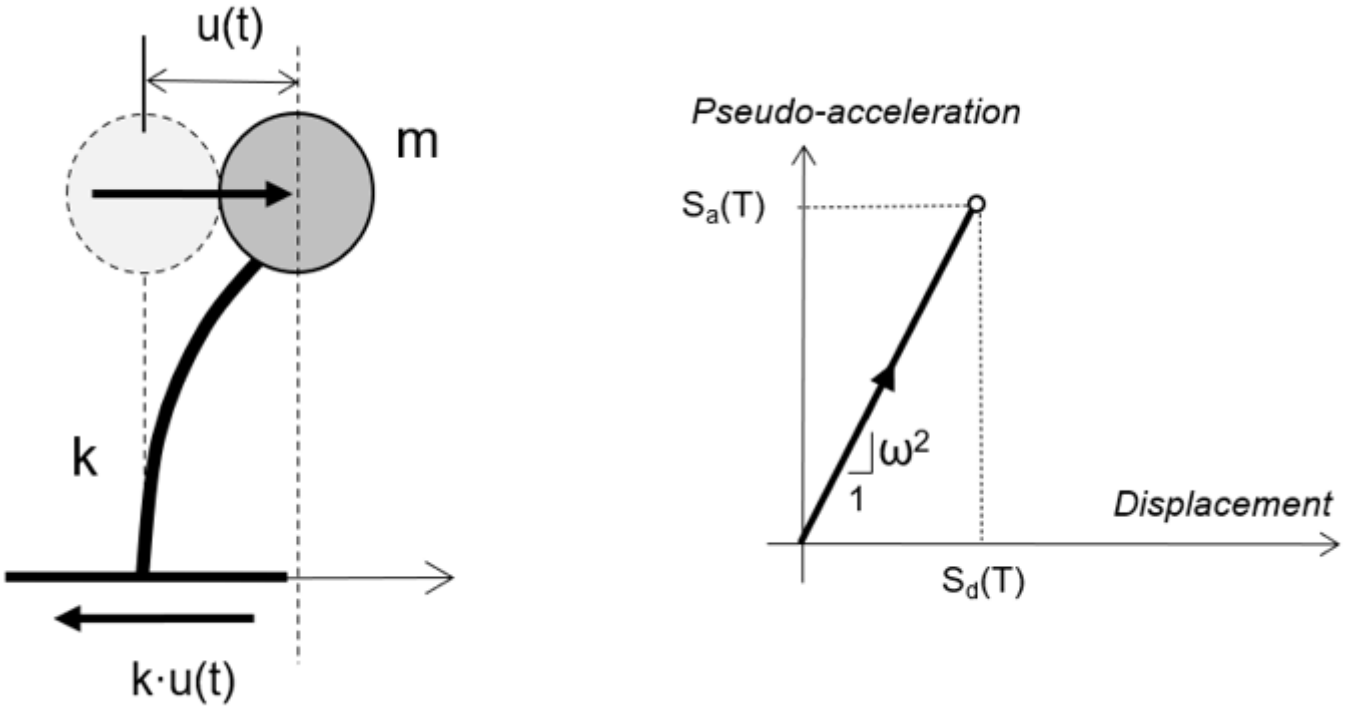

Figure 1

Characterization of the linear elastic SDOF and its response

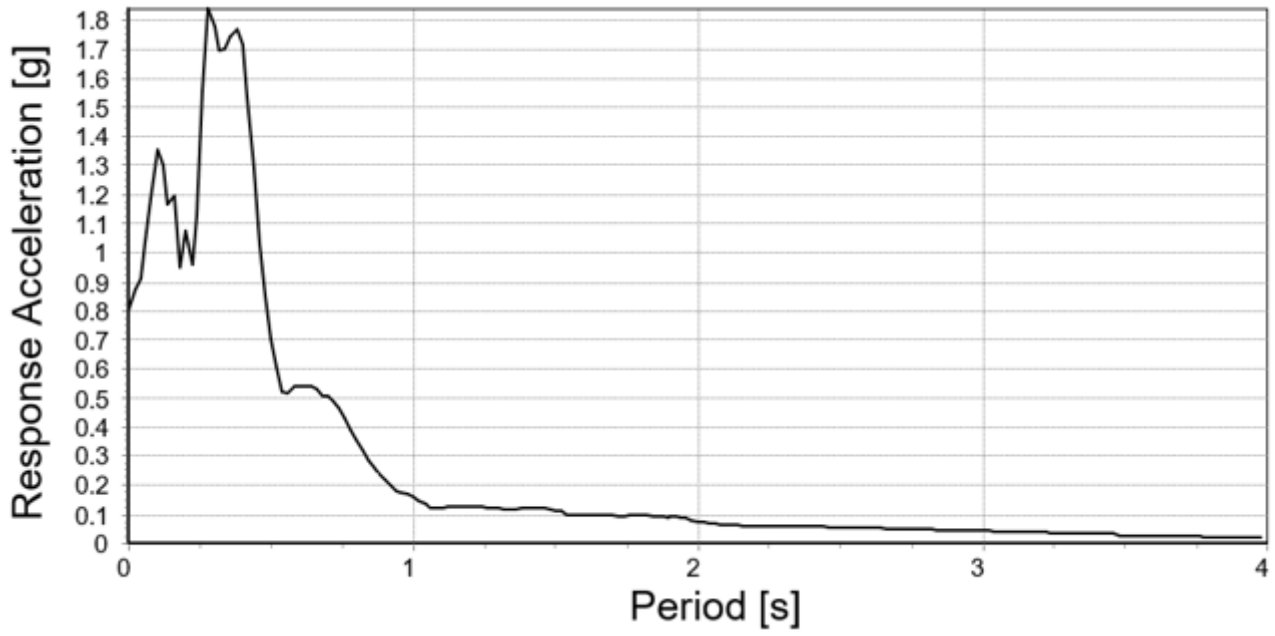

Figure 2

Pseudo-acceleration response spectra for the Corralitos record of the Loma Prieta Earthquake in October 17, 1989, for 5% damping.

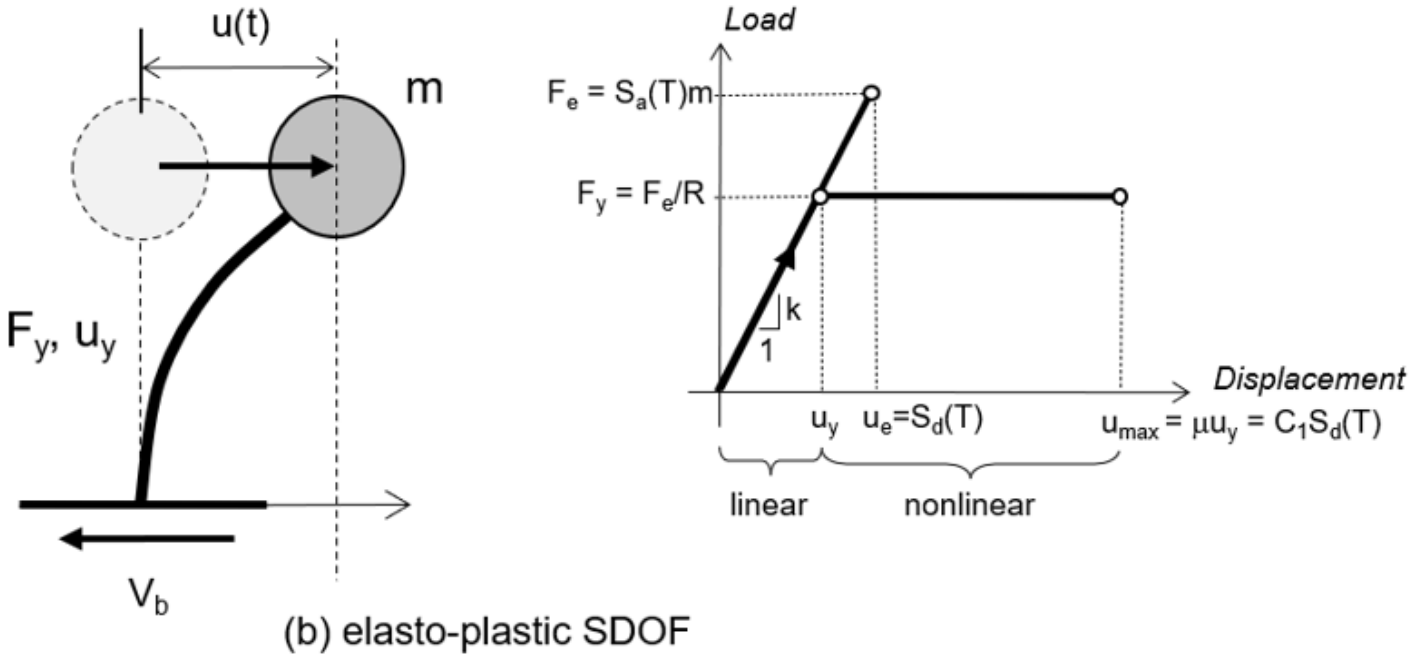

Figure 3

Characterization of the elasto-plastic SDOF and its response

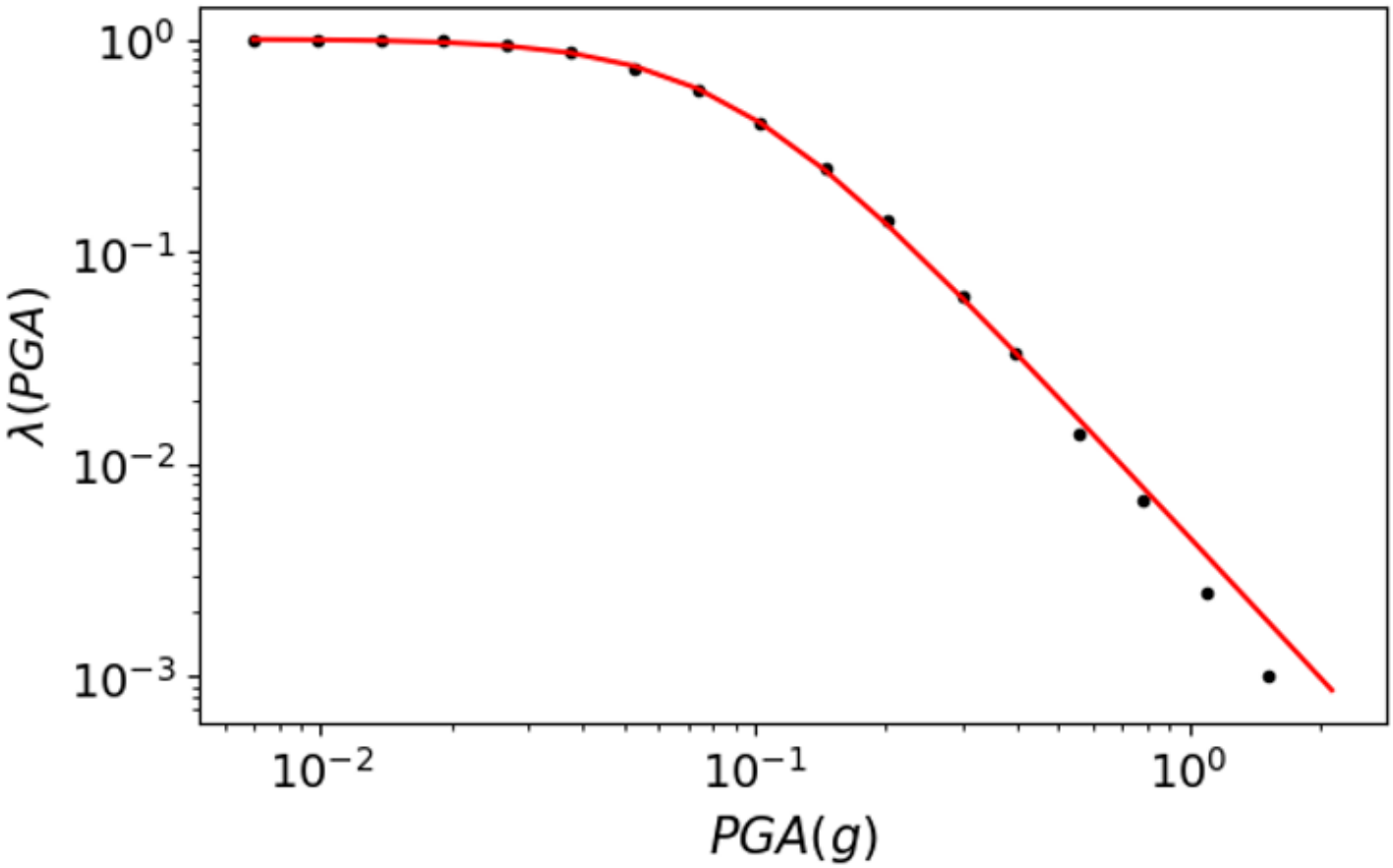

Figure 4

Seismic hazard curve (black dots) and the fitting model (red line). Granada (Spain), Vs_{30}=250m/s.

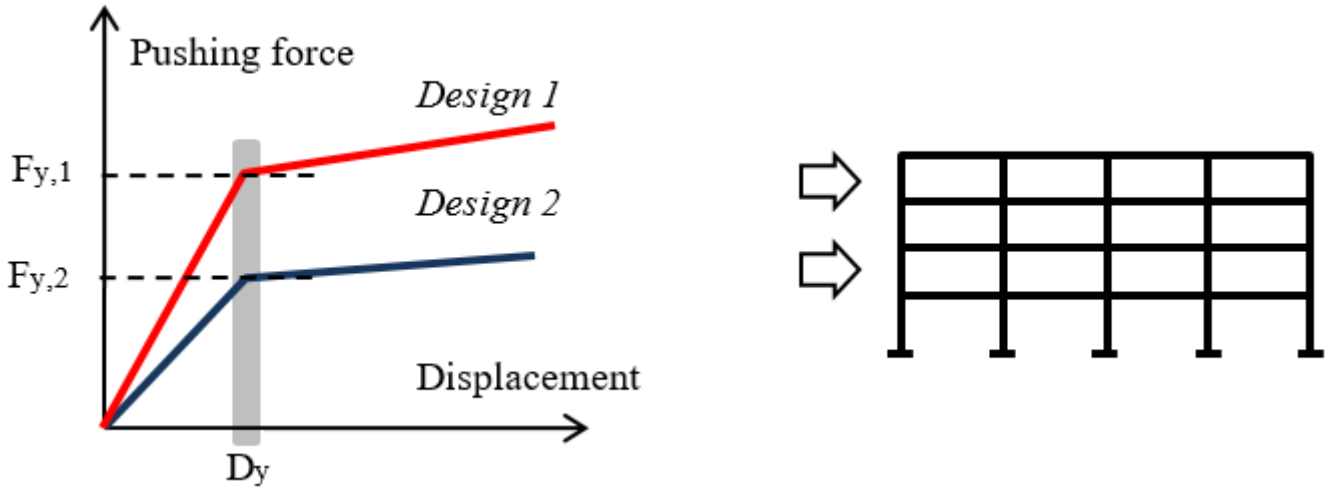

Figure 5

Yield displacement of two models that differ only in component reinforcement quantity.

Figure 6

Development of the Yield Frequency Spectra

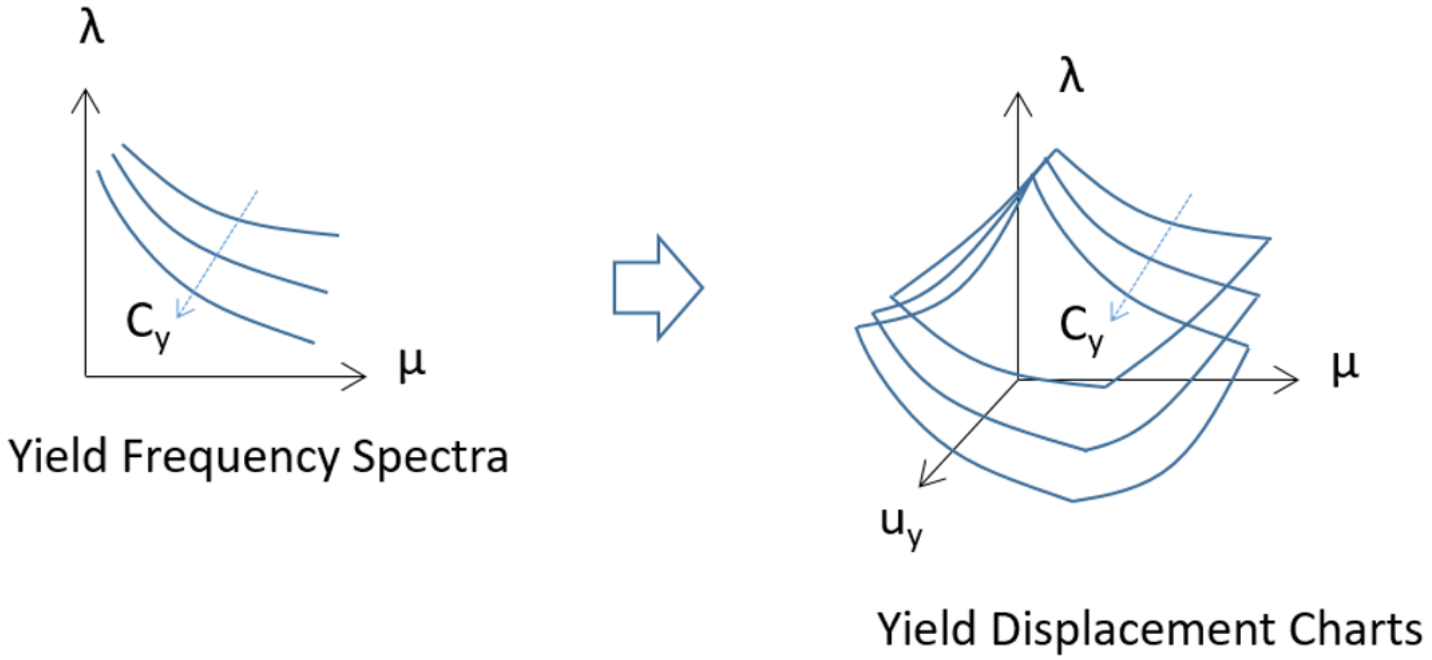

Figure 7

Yield Displacement Charts

Figure 8

u_{max} versus PGA (left) and its power-law relationship in logarithmic space (right) for the database of 980 ground motions (C_y=0.3, u_y=0.025m).

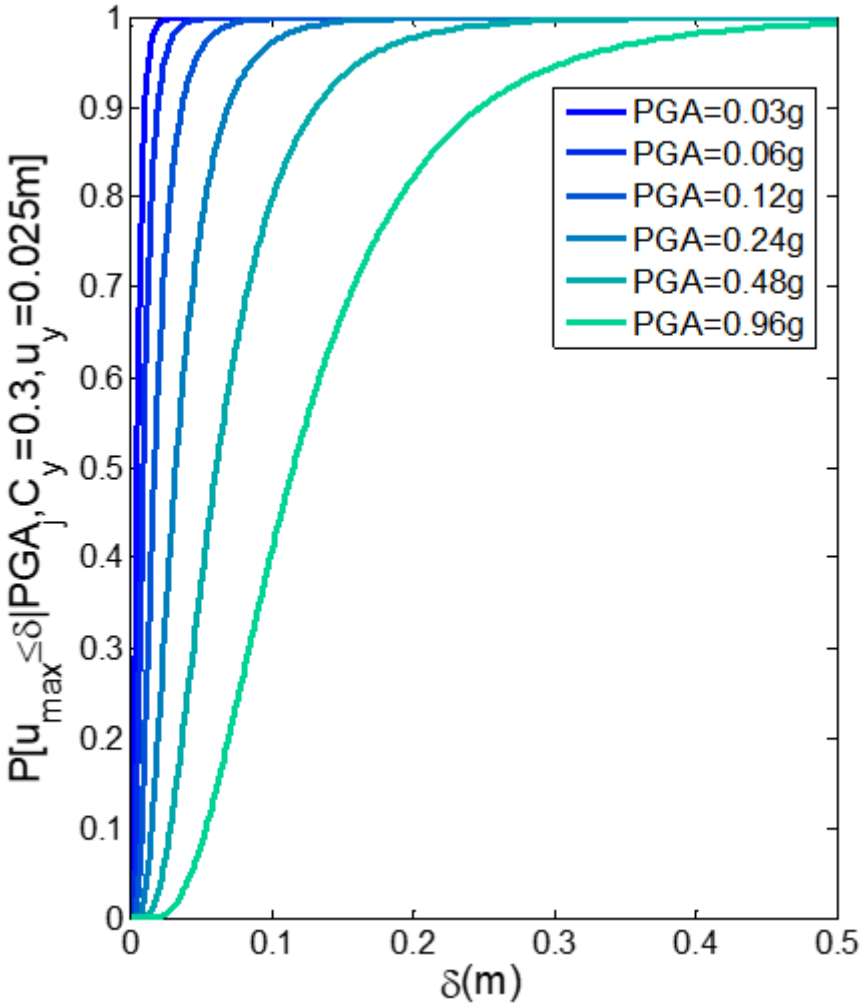

Figure 9

LogNormal Cumulative Distribution Function (μ=-2.12+0.92·ln(PGA), σ=0.6) for u_y=0.025 m, C_y=0.3, and different values of PGA.

Figure 10

λ-μ curve for u_y=0.025m, C_y=0.3, and the location in Granada

Figure 11

u_{max} versus *PGA* for different values of earthquakes and SDOF systems. (a) u_y=0.025m, (b) u_y=0.05m, (c) u_y=0.1m. C_y=0.1,...,1.

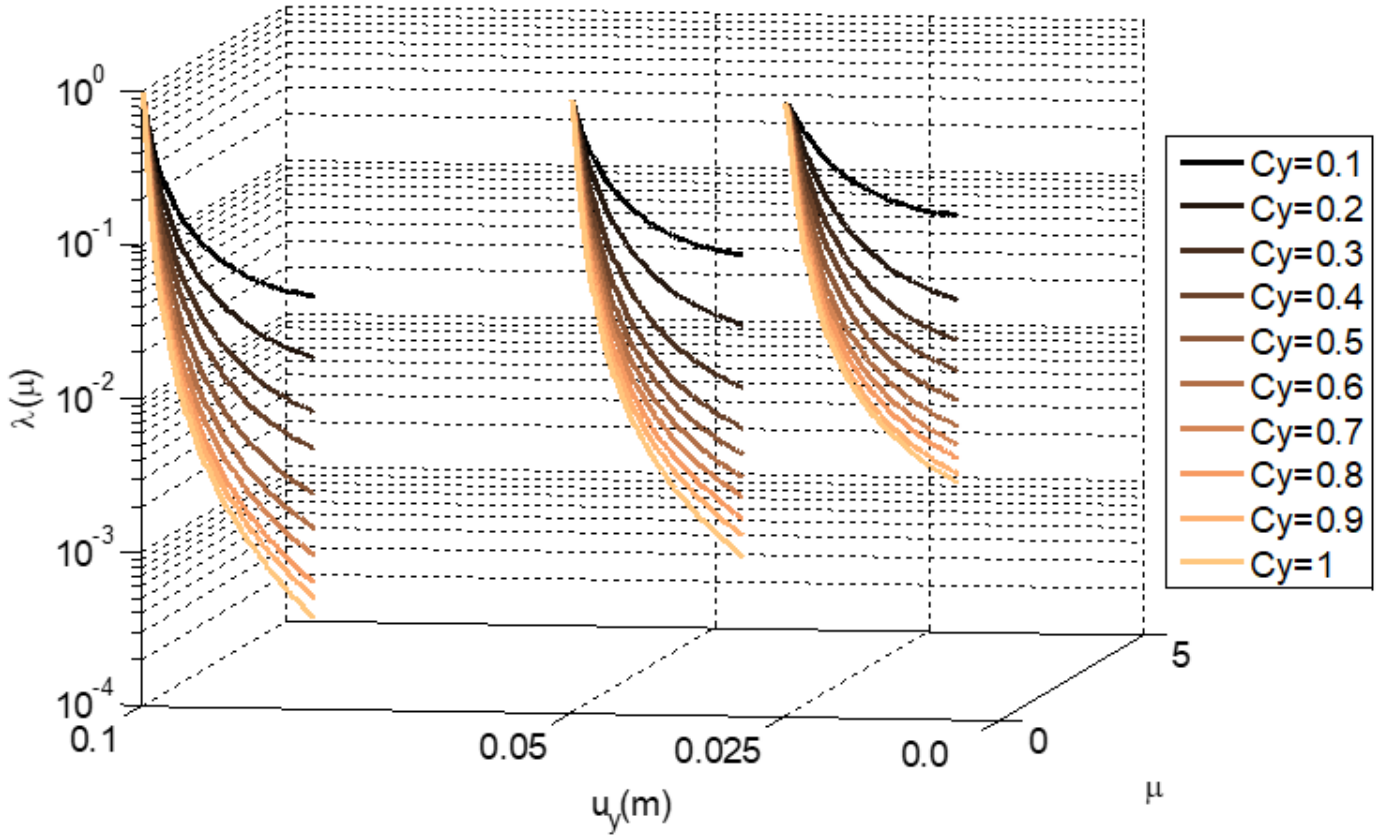

Figure 12

Yield Displacement Chart for the city of Granada.

Figure 13

Bridge column and single-degree-of-freedom model.

Figure 14

Yield displacement of a cantilever beam

Figure 15

YFS for u_y = 0.048 m and the two performance objectives.